Geomechanics and Engineering, *Vol. 17, No. 6 (2019) 583-595*
DOI: https://doi.org/10.12989/gae.2019.17.6.583

The effect of foundation soil behavior on seismic response of long bridges

Shima Sadat Hoseini*[1], Ali Ghanbari[1a], Mohammad Davoodi[2b] and Milad Kamal[1c]

[1]*Department of Civil Engineering, Kharazmi University, Moffateh Avenue, Tehran, Iran*
[2]*Department of Geotechnical Earthquake Engineering, International Institute of Earthquake Engineering and Seismology, Tehran, Iran*

(Received March 15, 2018, Revised March 11, 2019, Accepted March 22, 2019)

Abstract. In this paper, a comprehensive investigation of the dynamic response of a long-bridge subjected to spatially varying earthquake ground motions (SVEGM) is performed based on a proposed analytical model which includes the effect of soil-structure interaction (SSI). The spatial variability of ground motions is simulated by the powerful record generator, SIMQKE II. Modeling of the SSI in the system is simplified by replacing the pile foundations and soil with sets of independent equivalent linear springs and dashpots along the pile groups. One of the most fundamental objectives of this study is to examine how well the proposed model simulates the dynamic response of a bridge system. For this purpose, the baseline data required for the evaluation process is derived from analyzing a 3D numerical model of the bridge system which is validated in this paper. To emphasize the importance of the SVEGM and SSI, bridge responses are also determined for the uniform ground motion and fixed base cases. This study proposing a compatible analytical model concerns the relative importance of the SSI and SVEGM and shows that these effects cannot be neglected in the seismic analysis of long-bridges.

Keywords: SVEGM; SSI; dynamic response; long bridges; seismic analysis

1. Introduction

Effect of SSI and SVEGM have been two interesting keywords in seismic analysis of long structures in these decades.

Among the various methods to investigate the effect of SSI, the direct modeling of the soil-structure system potentially provides a more powerful means for obtaining realistic estimates of SSI.

The most common practical approach in soil-structure interaction modeling method is the spring-dashpot method in which the substructure soil replaces with the springs and dashpots. In recent decades, the spring-dashpot models have been widely used for simulating the soil-structure interaction effect (e.g., Rahmani *et al.* 2016). Pacheco *et al.* 2006 developed an analytical spring-dashpot model includes the soil contribution to the system inertial properties through a series of lumped mass, consistent with the Discrete Winkler model and defined the stiffness, damping, and mass coefficients according to the Poisson's ratio. Shirgir *et al.* (2016) studied the effect of SSI and dynamic performance of pile group supported bridges. An analytical model was proposed in their study to predict seismic analysis of the bridges.

Also, an analytical method has been used widely for SSI analyzing of the other structures such as foundations, reinforced slopes and elevated tanks (e.g., Varzaghandi and Ghanbari 2014, Ghanbari *et al.* 2013 and Maedeh *et al.* 2017).

Another important concept in dynamic analysis of long structures, such as long bridges is SVEGM which can change the dynamic response of the structures. Davoodi *et al.*, (2012 and 2013) investigate the effect of SVEGM on seismic response of embankment dams. Also, a large number of studies have been done to investigate the effect of SVEGM on the dynamic response of long bridges (e.g., Nazmy and Abdel-Ghaffar 1992, Wang *et al.* 2009, Karmakar *et al.* 2012, Apaydin and Harmandar 2016 and Adanur and *et al.* 2016). Some studies are available, which investigated the effect of both SSI and SVEGM on bridge systems. Bi *et al.* (2011), for example, studied the combined effects of SVEGM, local site amplification and SSI on bridge responses. The soil surrounding the pile foundation was modeled by frequency-dependent springs and dashpots. The peak structural responses were estimated using the standard random vibration method. Numerical results showed that SSI significantly affects the structural responses. Soyluk and Sicacik (2012) also studied the influence of SVEGM and SSI on the relative response of cable-stayed bridges. The substructure method was used in their analysis. It was calculated that both SSI and SVEGM effects should be considered in the dynamic analysis of these bridges. Sextos *et al.* (2003 (1, 2)) presented a parametric analysis aiming to study the sensitivity of bridge responses to SVEGM, site effects, and SSI. Based on the results of the comparative finite element analysis, it was concluded that the proposed method is a feasible and efficient way to generate more realistic earthquake motion scenarios than those commonly used and to account for the properties of the soil foundation-pier system under seismic loading.

*Corresponding author, Ph.D. Candidate
E-mail: hoseinishima1365@gmail.com
[a]Professor
[b]Associate Professor
[c]Master Student

ISSN: 2005-307X (Print), 2092-6219 (Online)

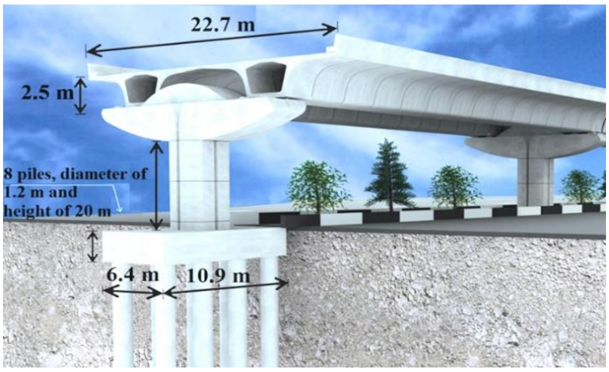

Fig. 1 Detailed view of Sadr Bridge

Fig. 2 Sadr Bridge view

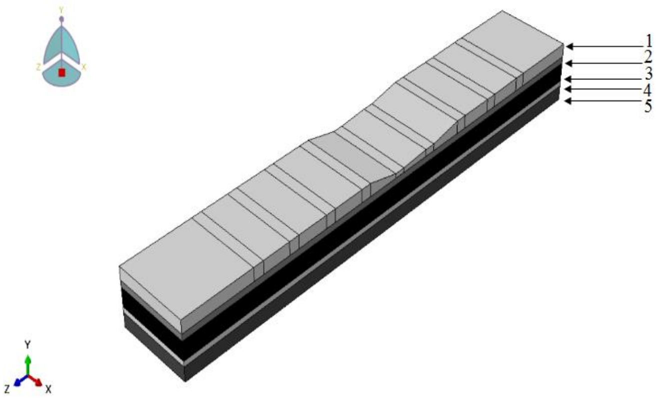

Fig. 3 Soil layers at the site

The focus of this paper is to present a new analytical model for long-span bridge systems subjected to SVEGM and under the effect of SSI. For this purpose, 350 m of Sadr high way bridge in Iran is simulated and analyzed. Nonlinear response of the foundation soil and the bridge piers are accounted for in the analysis using advanced constitutive model. The direct model is validated and then based on the validated direct model, detailed baseline data is generated for the bridge model. The bridge system is also analytically simulated using the spring-dashpot method. In the following sections, the direct and spring-dashpot models of the bridge system are first described, and the spring-dashpot model is evaluated by comparing the results with those obtained from the direct model. Then the effect of SVEGM on the dynamic response of the bridge is investigated by use of the adequate spring-dashpot method.

2. Description of the case study

The Sadr high way bridge is the longest high way bridge in Tehran, Iran which was built in 2013 as the 11th highest bridge in the world is selected as a case study in this paper. The piers of the main bridge are different in height but all of them are 3 m length and 3.2 m in width. The pier foundations are composed of a 6.4 m×10.9 m pile caps with a thickness of 2 m supported by 6×4 pile groups with a length of 20 m and diameter of 1.2 m (Fig. 1). In this study, a section of 346 m of the main bridge which is separated from the rest by two suitable expansion joints is selected to investigate the effect of SSI and SVEGM on the dynamic response of the highest section of Sadr Bridge. With these expansion joints, it could be possible to model the selected part of the bridge without considering the neighbor parts. This section of the bridge is of single-pier type and is in close proximity to the active faults of the region, which

Table 1 Properties of the soil layers

Parameter	Value				
	Layer 1	Layer 2	Layer 3	Layer 4	Layer 5
Thickness (m)	6	2	17	5	10
G (MPa) Shear modulus	60	275	175	275	175
c (kg/cm^2) Soil cohesion	0.17	0.19	0.16	0.21	0.18
φ° Soil friction angle	37	36	41	41	39
ρ (kg/m3) Soil density	1500	1800	1900	1800	1900
ψ° Dilation angle	7	6	11	5	9
Tensile stress	0	0	0	0	0
Deviatoric eccentricity(e)	0.66	0.67	0.64	0.68	0.65
Meridional eccentricity	0.1	0.1	0.1	0.1	0.1
Yield Stress (kg/cm2)	0.17	0.19	0.16	0.21	0.18
Plastic strain	0	0	0	0	0

have caused several earthquakes so far. Fig. 2 shows a view of the bridge. The properties of soil layers under the bridge structure are given in Table 1 and Fig. 3.

3. Description of the Sadr Bridge analytical model

Fig. 4 illustrates the schematic view of two largest decks of the Sadr Bridge standing on 9 piers and pile groups. Two decks with length of $d_1=d_2=173$ m are supported by 9 capitals which are connected to 9 piers standing on the pile foundations. The structure of the bridge continues on both sides and neighboring spans are separated from the considered structure by appropriate expansion joints. The decks are considered as lumped mass model with the total mass of $m_1=m_2=8177719.5$ kg. The concrete piers with height of $h_1=7.47$ m, $h_2=7.95$ m, $h_3=7.87$ m, $h_4=13.3$ m, $h_5=15.3$ m, $h_6=7.74$ m, $h_7=7.76$ m, $h_8=7.64$ m, and $h_9=7.58$ m are modeled with lateral stiffness of $kp_1=7.3\times10^9$ N/m, $kp_2=6\times10^9$ N/m, $kp_3=6.2\times10^9$ N/m, $kp_4=1.3\times10^9$ N/m, $kp_5=8.5\times10^9$ N/m, $kp_6=6.6\times10^9$ N/m, $kp_7=6.5\times10^9$ N/m, $kp_8=6.8\times10^9$ N/m, and $kp_9=7\times10^9$ N/m.

The most widely used model to perform the analysis of piles under lateral loads consists of modeling the piles as a series of beam elements and representing the soil as a group of unconnected, concentrated springs and dashpots perpendicular to the pile known as spring-dashpot method. The most important issue in this method is to determine the stiffness and damping ratio of springs and dashpots used to simulate the soil around the piles. In this study *p-y* nonlinear backbone curves are determined along the pile foundations following the guidelines of API (2007) to determine the nonlinear stiffness of the soil along the piles. To determine the group reduction factors to consider the effect of pile groups the guidelines of AASHTO (2012) are used. The load-deflection backbone curves for embedded pile caps are derived following the procedure presented by GEOSPECTRA (1997). In this procedure, the initial

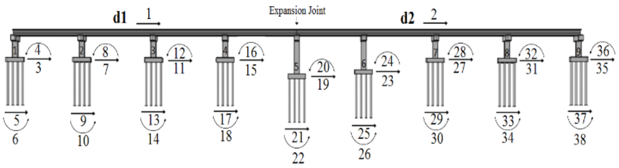

Fig. 4 Schematic view of two largest decks of the Sadr Bridge

stiffness is calculated assuming a passive wedge type failure in front of the pile cap. For the rotational stiffness coefficients, Gazetas equations were used as, $K_\theta = \frac{8G_{soil}r^3}{3(1-\nu_{soil})}$, and $K_{h\theta} = K_{\theta h} = \frac{0.56G_{soil}r^2}{2-\nu_{soil}}$, where r is radius of the equivalent circle foundation. The load deflection backbone curve suggested by GEOSPECTRA is given as, $F = \Delta/({}^{1}/_{K_{max}} + {}^{R_f}/_{F_p})$, where F is the load at deflection Δ, K_{max} is the initial stiffness of the pile cap, F_p is the force which is given by $R_f = 1 - {}^{F_p}/_{(K_{max}\Delta_{max})}$, where Δ_{max} is the deflection at the ultimate passive soil resistance. With the assumption of acting as a retaining wall Δ_{max} varies from 0.002h to 0.04h in which, h is the thickness of the pile cap. In this paper Δ_{max} is assumed to be 0.02h. Therefore, the stiffness matrix of the pile cap will be

$$[K_{cap}] = \begin{bmatrix} {}^{F}/_{\Delta} & K_{h\theta} \\ K_{\theta h} & K_\theta \end{bmatrix}$$

To determine the stiffness coefficients along the piles by use of the p-y backbone curves, depth-varying time histories of displacement in absence of the bridge structure is required. In order to achieve this purpose, nonlinear time history analysis is calculated using true nonlinear constitutive model in the computer program, ABAQUS (2011) (Fig. 3). The input ground motion is applied to the base of the soil profile in the form of displacements. The output is the depth-varying time histories of displacement in the free-field for the foundation soil and the corresponding maximum displacements (Δ_n) for each depth. With the values of Δ_n and nonlinear backbone curves, nonlinear stiffness along the pile-foundations are determined. The damping values are determined using the Rayleigh approach where the elements of the damping matrix are calculated as, $C_{ij} = \alpha M_{ij} + \beta K_{ij}$, where α, β are damping coefficients, M_{ij} are the elements of the mass matrix and K_{ij} are the elements of the stiffness matrix of the system. To obtain the values of α and β, equation of $\alpha + \beta\omega^2 = 2\omega_i\xi_i \Rightarrow \xi_i = 1/2(\frac{\alpha}{\omega_i} + \beta\omega_i)$ was written twice with two different ω. One of the most useable approach to determine the α and β with the above equation is to consider ω_1 and ω_2 as the predominant frequency of the input motion and the first free vibration frequency of the system. In this equation, ξ is damping ratio. Traditionally, the damping ratio of the bridge system is assumed to be 5% without considering the energy dissipation at the bridge supports (Lee *et al.* 2011). Werner 1993 reported damping ratios from 19% to 26% for bridge system by use of system identification techniques. Also, Lee *et al.* (2011) reported a damping ratio in both longitudinal and transverse directions as 25%. In this study, as recommended in the previous studies, the damping ratio is approximated to be 25%. This amount of damping lies in all ranges reported in the previous studies (i.e., Lee *et al.*, 2011, Wang *et al.*, 2009 and Werner 1993) and seems to be suitable for the systems in which the structural system and soil are considered together. So it could be written as

$$\xi = 0.25$$

$$\omega_1 = 11.18\ \text{rad/sec} \Rightarrow \begin{cases} \alpha = 0.48 \\ \beta = 5.1 \times 10^{-3} \end{cases}$$

$$\omega_2 = 8.48\ rad/se$$

Under these assumptions, the bridge system can be modelled as a thirty eight degrees of freedom in order to investigate the effect of SSI and SVEGM on seismic response of the system as shown in Fig. 4.

4. Analytical solution of the dynamic equilibrium equation

In the present study, the dynamic response of the long span bridge shown in Fig. 4 is calculated. Firstly, equation of motion is solved in frequency domain, then by use of inverse Fourier transformation responses are derived in time domain. The equivalent spring-dashpot method is used to analysis SSI effect. In this method, the super structure and the foundation medium, are treated as two independent models. The connection between the two models is established by the interaction forces acting on the interface. The dynamic equilibrium equations are finally written in terms of interface degrees of freedom. With this background, the dynamic equilibrium equations can be expressed in the matrix form as follows

$$\begin{bmatrix} M_{ss} & M_{sf} \\ M_{fs} & M_{ff} \end{bmatrix}\begin{Bmatrix} \ddot{u}_s^t \\ \ddot{u}_f^t \end{Bmatrix} + \begin{bmatrix} C_{ss} & C_{sf} \\ C_{fs} & C_{ff} \end{bmatrix}\begin{Bmatrix} \dot{u}_s^t \\ \dot{u}_f^t \end{Bmatrix} + \begin{bmatrix} K_{ss} & K_{sf} \\ K_{fs} & K_{ff} \end{bmatrix}\begin{Bmatrix} u_s^t \\ u_f^t \end{Bmatrix} = \begin{Bmatrix} 0 \\ P_f^t \end{Bmatrix} \quad (1)$$

in which [*M*], [*C*] and [*K*] are the mass, damping and stiffness matrices, respectively, $\{\ddot{u}\}$, $\{\dot{u}\}$ and $\{u\}$ are the acceleration, velocity and displacement vectors, respectively and $\{P_f^t\}$ is the total nodal forces vector at the base degree of freedom. The subscripts *s* and *f* refer to the super structure and the foundation, respectively (Datta 2010).

The total displacement is written as the sum of two displacement components of quasi-static and dynamic displacement vectors

$$\begin{Bmatrix} u_s^t \\ u_f^t \end{Bmatrix} = \begin{Bmatrix} u_s^d \\ u_f^d \end{Bmatrix} + \begin{Bmatrix} u_s^{qs} \\ u_g \end{Bmatrix} \quad (2)$$

where u_f^d is the interaction displacement vector at the structure-foundation contact points and u_g is the corresponding free field ground motion vector. To define the quasi-static displacement Eq. (2) substitutes into Eq. (1) and all the dynamic terms are put zero, then

$$[u_s^{qs}] = -[K_{ss}^{-1}][K_{sf}]\{u_g\} = \frac{1}{\omega^2}[K_{ss}^{-1}][K_{sf}]\{\ddot{u}_g\} \quad (3)$$

Eq. (1) can be expressed in the frequency domain as

$$[Z(i\omega)]\{u^d(i\omega)\} = [Z_g(i\omega)]\{u_g(i\omega)\} \quad (4)$$

where

$$\{u(i\omega)\} = \{u_1(i\omega)u_2(i\omega)u_3(i\omega)\ \varphi_4(i\omega)u_5(i\omega)\ \varphi_6(i\omega)u_7(i\omega)\ \varphi_8(i\omega)u_9(i\omega)\varphi_{10}(i\omega)u_{11}(i\omega)\varphi_{12}(i\omega)u_{13}(i\omega)\varphi_{14}(i\omega)\ u_{15}(i\omega)\varphi_{16}(i\omega)u_{17}(i\omega)\varphi_{18}(i\omega)u_{19}(i\omega)\varphi_{20}(i\omega)u_{21}(i\omega)\ \varphi_{22}(i\omega)u_{23}(i\omega)\varphi_{24}(i\omega)u_{25}(i\omega)\varphi_{26}(i\omega)u_{27}(i\omega)\varphi_{28}(i\omega)\ u_{29}(i\omega)\varphi_{30}(i\omega)u_{31}(i\omega)\varphi_{32}(i\omega)u_{33}(i\omega)\varphi_{34}(i\omega)u_{35}(i\omega)\ \varphi_{36}(i\omega)u_{37}(i\omega)\varphi_{38}(i\omega)\}^T$$

and

$$\{u_g(i\omega)\} = \{u_{g1}(i\omega)u_{g2}(i\omega)u_{g3}(i\omega)\ u_{g4}(i\omega)u_{g5}(i\omega)\ u_{g6}(i\omega)u_{g7}(i\omega)\ \ u_{g8}(i\omega)u_{g9}(i\omega)\}^T$$

are defined as the dynamic response vector and the input ground motion vector, respectively. $[Z(i\omega)]$ and $[Z_g(i\omega)]$ are the impedance matrices of the dynamic system.

$$[Z(i\omega)] = \begin{bmatrix} z_{1\,1}(i\omega) & \cdots & z_{1\,38}(i\omega) \\ \vdots & \ddots & \vdots \\ z_{38\,1}(i\omega) & \cdots & z_{38\,38}(i\omega) \end{bmatrix} \quad (5)$$

$$[Z_g(i\omega)] = \begin{bmatrix} z_{g1\,1}(i\omega) & \cdots & z_{g19}(i\omega) \\ \vdots & \ddots & \vdots \\ z_{g38\,1}(i\omega) & \cdots & z_{g38\,9}(i\omega) \end{bmatrix} \quad (6)$$

in which

$$z_{ij}(i\omega) = -\omega^2 M_{ij} + i\omega C_{ij} + K_{ij} \quad (7)$$

where, M_{ij}, C_{ij} and K_{ij} are the mass, damping coefficient and stiffness corresponded to each element, respectively.

To obtain the stiffness matrix three consecutive steps is used as following:

1. Calculation of the pile group stiffness matrix ($[K_b]$) as:

With considering Battini's (2006) shape functions pile group stiffness matrix can be calculated (Fig. 5).

$$[K_b] = n \times m \int_0^l EI[N''(x)]^T[N''(x)]\,dx \quad (8)$$

$$[N(x)]^T = \left[1 - \frac{3x^2}{L^2} + \frac{2x^3}{L^3} \quad x(1-\frac{x}{L})^2 \quad 3\frac{x^2}{L^2} - 2\frac{x^3}{L^3} \quad \frac{x^2(\frac{x}{L}-1)}{L}\right] \quad (9)$$

$$[K_b] = n \times m \begin{bmatrix} \frac{12EI}{L^3} & \frac{6EI}{L^2} & \frac{-12EI}{L^3} & \frac{6EI}{L^2} \\ \frac{6EI}{L^2} & \frac{4EI}{L} & \frac{-6EI}{L^2} & \frac{2EI}{L} \\ \frac{-12EI}{L^3} & \frac{-6EI}{L^2} & \frac{12EI}{L^3} & \frac{-6EI}{L^2} \\ \frac{6EI}{L^2} & \frac{2EI}{L} & \frac{-6EI}{L^2} & \frac{4EI}{L} \end{bmatrix} \quad (10)$$

where [*N*] is the shape function vector, *E* is the Young's modulus of piles, *I* is the cross sectional moment of inertia, L is the pile's length, and $n \times m$ is the piles number in the group.

2. Calculation of the pile surrounding soil stiffness matrix ($[K_s]$) as

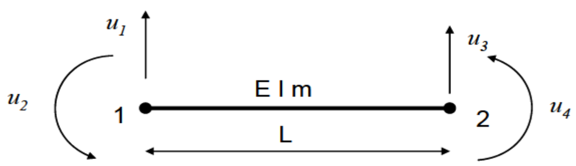

Fig. 5 Degrees of freedom considered for the pile elements

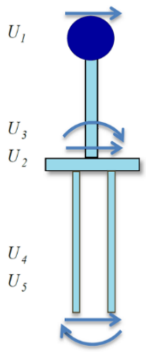

Fig. 6 Structural system stood on a pile group

$$[K_b] = n \times m \begin{bmatrix} \frac{12EI}{L^3} & \frac{6EI}{L^2} & \frac{-12EI}{L^3} & \frac{6EI}{L^2} \\ \frac{6EI}{L^2} & \frac{4EI}{L} & \frac{-6EI}{L^2} & \frac{2EI}{L} \\ \frac{-12EI}{L^3} & \frac{-6EI}{L^2} & \frac{12EI}{L^3} & \frac{-6EI}{L^2} \\ \frac{6EI}{L^2} & \frac{2EI}{L} & \frac{-6EI}{L^2} & \frac{4EI}{L} \end{bmatrix} \tag{11}$$

$$[K_s'] = \sum_{i=1}^{l} K_i [N^{"}(x)]^T [N^{"}(x)] \tag{12}$$

$$[K_s] = \sum_{j=1}^{n} ma_j \begin{bmatrix} \frac{13}{35}\sum K_i & \frac{11}{210}L\sum K_i & \frac{9}{70}\sum K_i & -\frac{13}{420}L\sum K_i \\ \frac{11}{210}L\sum K_i & \frac{1}{105}L^2\sum K_i & \frac{13}{420}L\sum K_i & -\frac{1}{140}L^2\sum K_i \\ \frac{9}{70}\sum K_i & \frac{13}{420}L\sum K_i & \frac{13}{35}\sum K_i & -\frac{11}{210}L\sum K_i \\ -\frac{13}{420}L\sum K_i & -\frac{1}{140}L^2\sum K_i & -\frac{11}{210}L\sum K_i & \frac{1}{105}L^2\sum K_i \end{bmatrix}$$
$$= \begin{bmatrix} \frac{13}{35}K_a & \frac{11}{210}K_aL & \frac{9}{70}K_a & -\frac{13}{420}K_aL \\ \frac{11}{210}K_aL & \frac{1}{105}K_aL^2 & \frac{13}{420}K_aL & -\frac{1}{140}K_aL^2 \\ \frac{9}{70}K_a & \frac{13}{420}K_aL & \frac{13}{35}K_a & -\frac{11}{210}K_aL \\ -\frac{13}{420}K_aL & -\frac{1}{140}K_aL^2 & -\frac{11}{210}K_aL & \frac{1}{105}K_aL^2 \end{bmatrix} \tag{13}$$

where, K_i is nodal stiffness according to API recommendation, l is the number of nodes considered along the piles, and a_j is the pile group reduction factor.

3. Calculation of the cap stiffness matrix ($[K_{cap}]$) as

$$[K_{cap}] = \begin{bmatrix} F/_{\Delta} & 0.56Gr^2/_{(2-\upsilon)} \\ 0.56Gr^2/_{(2-\upsilon)} & 8Gr^3/_{3(1-\upsilon)} \end{bmatrix} \tag{14}$$

4. Calculation of the soil-pile structure stiffness matrix as:

For a structural system on the pile group (Fig. 6) stiffness matrix can be calculated as follows

$$[K] = \begin{bmatrix} k_{11} & k_{12} & k_{13} & k_{14} & k_{15} \\ k_{21} & k_{22} & k_{23} & k_{24} & k_{25} \\ k_{31} & k_{32} & k_{33} & k_{34} & k_{35} \\ k_{41} & k_{42} & k_{43} & k_{44} & k_{45} \\ k_{51} & k_{52} & k_{53} & k_{54} & k_{55} \end{bmatrix} \tag{15}$$

where

$k_{11}, k_{21} = K_{st}$, $k_{12} = -K_{st}$, $k_{13}, k_{31} = -K_{st}h$, $k_{14}, k_{15}, k_{41}, k_{51} = 0$, $k_{22} = \frac{12nmEI}{L^3} + \frac{13K_a}{35} + K_{st} + \frac{F}{\Delta}$, $k_{23} = \frac{6nmEI}{L^2} + \frac{11}{210}K_aL + K_{st}h + \frac{0.56Gr^2}{(2-\upsilon)}$, $k_{24} = -\frac{12nmEI}{L^3} + \frac{9}{70}K_a$, $k_{25} = \frac{6nmEI}{L^2} - \frac{13}{420}K_aL$, $k_{32} = \frac{6nmEI}{L^2} + \frac{11}{210}K_aL + K_{st}h + \frac{0.56Gr^2}{(2-\upsilon)}$, $k_{33} = \frac{4nmEI}{L} + \frac{1}{105}K_aL^2 + K_{st}h^2$, $k_{34} = -\frac{6nmEI}{L^2} + \frac{13}{420}K_aL$, $k_{35} = \frac{12nmEI}{L} - \frac{1}{140}K_aL^2$, $k_{42} = -\frac{12nmEI}{L^3} + \frac{9}{70}K_a$, $k_{43} = -\frac{6nmEI}{L^2} + \frac{13}{420}K_aL$, $k_{44} = \frac{12nmEI}{L^3} + \frac{13K_a}{35}$, $k_{45} = -\frac{6nmEI}{L^2} - \frac{11}{210}K_aL$, $k_{52} = \frac{6nmEI}{L^2} - \frac{13}{420}K_aL$, $k_{53} = \frac{12nmEI}{L} - \frac{1}{140}K_aL^2$, $k_{54} = -\frac{6nmEI}{L^2} - \frac{11}{210}K_aL$, $k_{55} = \frac{4nmEI}{L} + \frac{1}{105}K_aL^2$

and

K_{st}, is the lateral stiffness of the structure, and h is the height of the structure from the base. The above matrix is used for a five degrees of freedom model as shown in Fig. 6. By developing this matrix and assembling the stiffness elements for a 38 degrees of freedom model (Fig. 4) the stiffness matrix for the proposed model can be derived.

The mass matrix of the system is written as proposed by Pacheco (2007)

$$[M] = \begin{bmatrix} m_s & 0 & 0 & 0 & 0 \\ 0 & \frac{13}{35}\overline{m}L & \frac{11}{210}\overline{m}L^2 & \frac{9}{70}\overline{m}L & -\frac{13}{420}\overline{m}L^2 \\ 0 & \frac{11}{210}\overline{m}L^2 & \frac{1}{105}\overline{m}L^3 & \frac{13}{420}\overline{m}L^2 & -\frac{1}{140}\overline{m}L^3 \\ 0 & \frac{9}{70}\overline{m}L & \frac{13}{420}\overline{m}L^2 & \frac{13}{35}\overline{m}L & -\frac{11}{210}\overline{m}L^2 \\ 0 & -\frac{13}{420}\overline{m}L^2 & -\frac{1}{140}\overline{m}L^3 & -\frac{11}{210}\overline{m}L^2 & \frac{1}{105}\overline{m}L^3 \end{bmatrix} \tag{16}$$

$$\overline{m} = n \times m \times \rho_{pile} \times A_{pile} + n \times m \times \rho_{soil} \times A_{pile} \times \alpha_m \tag{17}$$

where m_s is the structural mass, ρ_{pile} is the pile density, A_{pile} is the pile cross area, and α_m is the mass coefficient defined by Pacheco (2007). Mass matrix for the 38 degrees of freedom model can be calculated as explained above.

The damping matrix is calculated according the Rayleigh approach as explained above.

Finally, the dynamic response of the bridge structure can then be derived by substituting the mass, stiffness and damping matrices in the Eqs. (5) and (6) and calculating the dynamic equilibrium equation in frequency domain as below

$$\{u(i\omega)\} = [Z(i\omega)]^{-1}[Z_g(i\omega)]\{u_g(i\omega)\} \tag{18}$$

In order to obtain dynamic response in time domain, fast Fourier transformation is applied.

5. Spatially varying earthquake ground motion simulation

The programs SIMQKE I and SIMQKE II were used in this study to simulate SVEGM along the bridge supports. One of the most important factors in earthquake records generation is to produce power spectral density function, compatible with ground accelerations for desired soil condition. The program SIMQKE I is used to generate target spectral density function from a response spectra. In this study the target response spectra is Northridge - 1994 earthquake response spectra. This power spectral density function is given to SIMQKE II as an input data. SIMQKE II as a conditioned earthquake ground motion simulator is designed to generate an array of different spatially correlated earthquake ground motion at an arbitrary set of points, optionally statistically compatible with known or prescribed motions at other locations.

This program is also used in unconditional mode. Unlike conditional mode in which generated ground motions are statistically compatible with, or conditioned by, recorded ground motions at nearby point, in unconditional mode the ground motions are simulated using only the user prescribed space-time statistics. Supplied with a target ground motion spectral density function, which may be evolutionary in nature, the program employs covariance matrix decomposition in the frequency domain followed by best linear unbiased estimation and an inverse fast Fourier transform to efficiently produce the nonstationary, spatially correlated, conditioned or unconditioned ground motions. Complete details of the non-uniform ground motion generation can be found in authors' previous paper 2017.

6. Numerical modeling and validity

In the following the finite element model of the bridge developed using ABAQUS finite element program (2011) is described. Solid elements with extrude method are used to model the solid domain and the bridge system. All components of the Sadr Bridge including nine 6×4 pile-groups underneath the piers, nine piers, two decks and the supporting soil domain are modeled in a unified constitutive model. To connect pile-elements to the surrounding soil elements, embedded region technique considering the friction coefficient between the soil domain and pile groups is used. Connection between the pile caps and the surrounding and underneath soil are considered by use of tangential and frictionless interaction model respectively.

To identify the different soil layers, the soil profile is partitioned in the part modulus of ABAQUS.

In this model 50424 nodes and 46914 elements are used. 29472 elements were linear wedge elements of type C3D6 and 17442 elements were linear hexahedral elements of type C3D8R. Size of the elements in the soil profile was 5m but in the structural elements size was different. Lateral and down boundaries was considered free field and fixed.

Hysteretic nonlinear behavior of soil layers is simulated using an elasto-plastic constitutive model. The model includes a Drucker-Prager yield surface with a non-associative flow rule and a deviatoric kinematic hardening rule. This model was successfully used in previous studies to simulate soil-foundation-structure interaction problems such as pile foundation (e.g., Ilankatharan and Kutter 2008), and bridges (e.g., Kwon and Elnashai 2008). The input soil parameters for the constitutive model were adopted from the results of field tests and laboratory tests performed as a part of the Sadr Bridge construction project. These parameters are shown in Table 1.

Elastic behavior is assigned to the piles, the concrete pile caps, and the deck because in seismic design of bridge systems these elements are capacity-protected so that damage is not allowed. The bridge piers are usually allowed to yield since any possible damage can easily be detected and repaired. Concrete damaged plasticity model which is used in recently studies (e.g, Mander *et al.* 1988, Pulinska and Czerba 2013, Hany and Hantouche 2016, Chi *et al.* 2017 and Drygala *et al.* 2017) is used to account for the nonlinearity of the reinforced concrete of the piers. This model can be used both explicitly and implicitly and can

Table 2 Input parameters for the concrete material (Rahmani *et al.* 2016)

Parameters	Confined concrete	Unconfined concrete
f'_c , compressive strength (kPa)	34474	276000
ε_c, strain at compressive strength	0.004	0.002
f'_{cu} , crushing strength (kPa)	210000	0
ε_{cu}, strain at crushing strength	0.0014	0.008

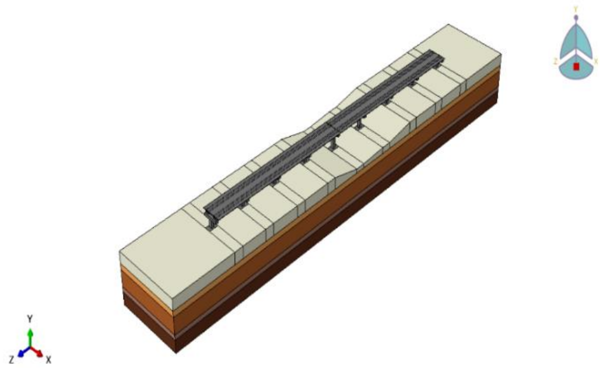

Fig. 7 Intended model for dynamic analysis

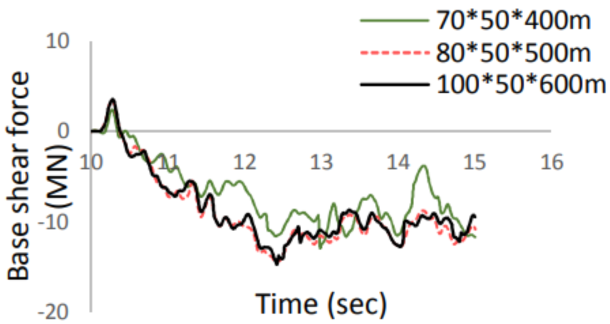

Fig. 8 Sensitivity of the shear force induced at the first pier base to the model dimensions

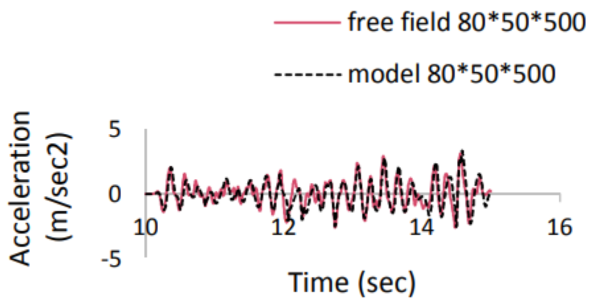

Fig. 9 Acceleration TH on top of the soil column compared to that at a point next to the lateral boundaries of the soil-bridge constitutive model on the ground surface

also simulate the cyclic behavior of concrete. It should be noted that the failure criterion of this behavioral model is defined by Drucker-Prager and its yield function is Lubliner (Drucker and Prager 1952 and Lubliner *et al.* 1989). Table 2 present the input parameters for the constitutive modeling of structural elements.

The first important step in analysis process is to detect the lateral boundaries. They should be placed at a location where the effects due to the presence of the bridge are negligible, and also free-field conditions at the lateral boundaries of the finite element model should be captured. To this end, three soil domain dimensions (70×50×300 m, 80×50×400 m, and 90×50×500 m in directions x, y, z shown in Fig. 7) are modeled and dynamic analysis are performed for them. The tenth to fifteenth seconds of the 1992 Landers earthquake with PGA of 0.78g, i.e., the portion of the motion including the PGA, is applied to the base of the model. To minimize the effects of the lateral boundaries on the seismic response of the bridge, the time histories of shear force at the first pier base are compared in Fig. 8. The comparison shows almost no difference between the results of the second and third models. To make sure that free field conditions at the lateral boundaries are appropriately captured, the soil response at these boundaries is investigated. To this end, two soil profile (50×80×500 m), one with the presence of bridge and the other one without the structure representing the foundation soil are subjected to the same ground motion at the base as a above. The resulting acceleration time histories at a point next to the lateral boundaries of these two model on the ground surface are compared to each other. Time history results (TH) in Fig. 9 show that the soil domain dimensions of 80×50×500 m properly captures the free field conditions. Accordingly, these intended dimensions are sufficient for the analysis.

To confirm the results of this numerical model, time history of the recorded earthquake at the ground surface should be retrieved at a depth of 20 m before applying at the base of the model. Retrieval process was performed by the equivalent linear program PROSHAKE (EduPro 2003). Therefore, a 20 m deep soil column is modeled in PROSHAKE with comparable properties to those in the free-field of the model. It means the same density of profile and shear wave velocity, representative modulus reduction and damping curve were considered and the recorded earthquake ground motion in the free-field is applied as outcrop motion to the surface of soil column in the PROSHAKE model. The resulting motion at the base of the PROSHAKE model is applied in the form of displacement time history to the base of the ABAQUS model. To avoid resulting different computed motion at the ground surface in the free-field of the ABAQUS model from the corresponding recorded one, iterative process is used for estimation of the modulus reduction and damping curve of the soil profile in the PROSHAKE model (Seed and Idriss 1970 and Sun *et al.* 1986).

Time history of the recorded and computed acceleration from the last iteration at the ground surface for the 1994 Northridge earthquake is presented in Fig. 10. The comparison shows that this retrieved ground motion can be used as appropriate input motion for the analysis. Fig. 11 shows the displacement response spectra at the lateral boundaries in the free-field of the ABAQUS model. It implies that a quite good agreement between the displacement response spectra of the recorded and computed motion is available. It means that the numerical model is generally capable of simulating the seismic responses of the considered system.

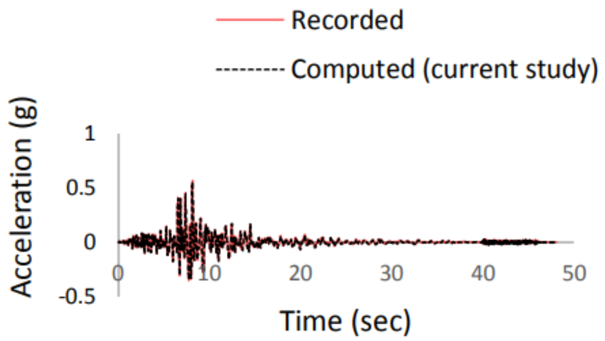

Fig. 10 Recorded and computed accelerations TH at the ground surface

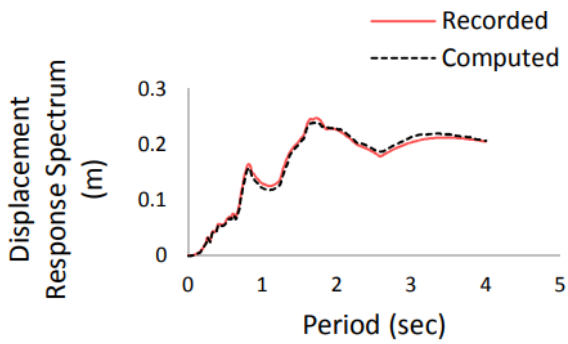

Fig. 11 Displacement response spectrum of motion for the damping ratio of 5% at the lateral boundaries

7. Results and discussion

In this study, it is intended to determine the effect of SSI and SVEGM on the seismic response of a long bridge model. To this end, the soil around the pile groups was replaced with equivalent springs and dashpots and also ground motion time histories are generated for non-uniform ground motion excitation. Dynamic response of the Sadr Bridge is determined in longitudinal and transverse directions for the models including and excluding the SSI and SVEGM effects. Relying on the validated numerical model, the results of this section are compared to those achieved by the validated model. Figs. 12 to 14 show the computed time histories of the first deck relative displacements with respect to the ground surface using the numerical and analytical models during the three earthquake events including the effect of SSI and excluding the effect of SVEGM. The figure illustrates that the variation of the first deck relative displacements over time is truly calculated in both longitudinal and transverse directions. Of course, the results for the Northridge, 1994 and Chi Chi, 1999 are not as precise as El Centro, 1979. It occurs because of the near-fault effect of those events. Due to the similarity of the responses of deck1 and deck2, only responses of deck1 are presented in this section.

Figs. 15 to 17 and Figs. 18 to 20 compare the

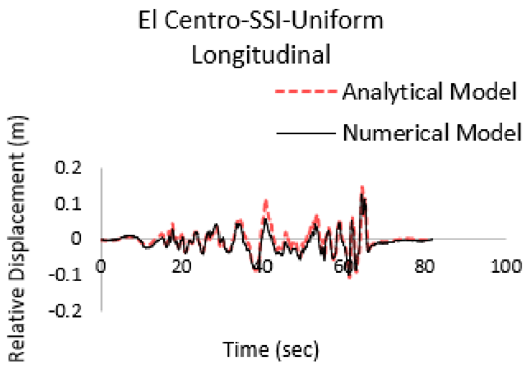

(a)

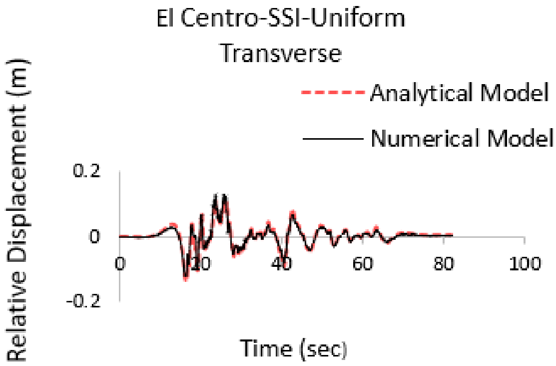

(b)

Fig. 12 The first deck relative displacements TH with respect to the ground surface for the 1979 El Centro earthquake in the (a) longitudinal and (b) transverse directions

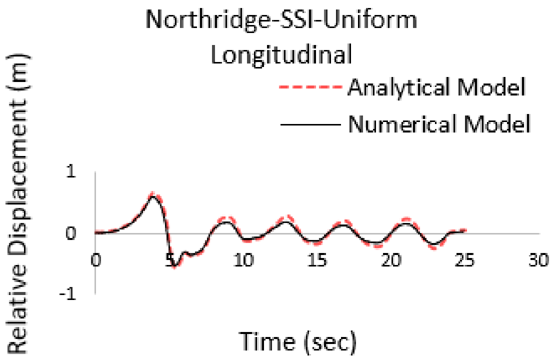

(a)

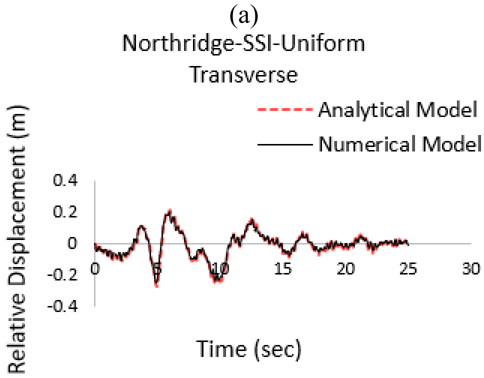

(b)

Fig. 13 The first deck relative displacements TH with respect to the ground surface for the 1994 Northridge earthquake in the (a) longitudinal and (b) transverse directions

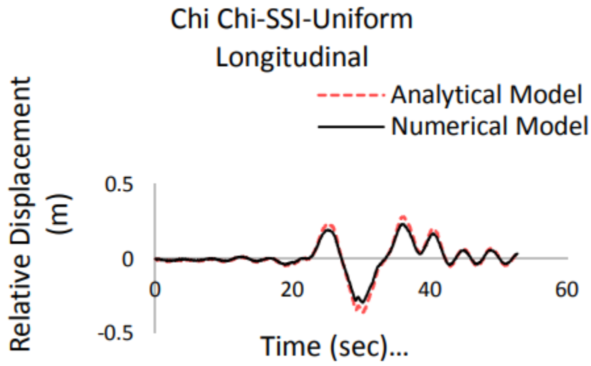

(a)

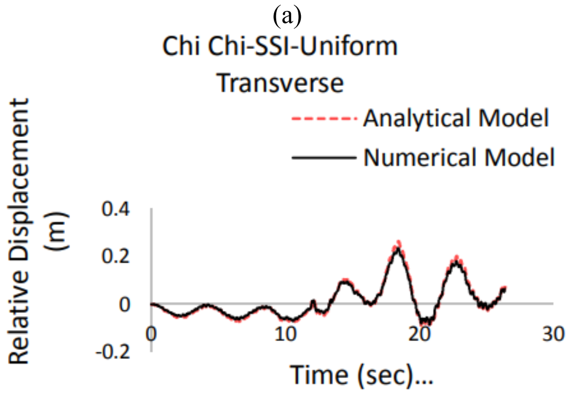

(b)

Fig. 14 The first deck relative displacements TH with respect to the ground surface for the 1999 Chi Chi earthquake in the (a) longitudinal and (b) transverse directions

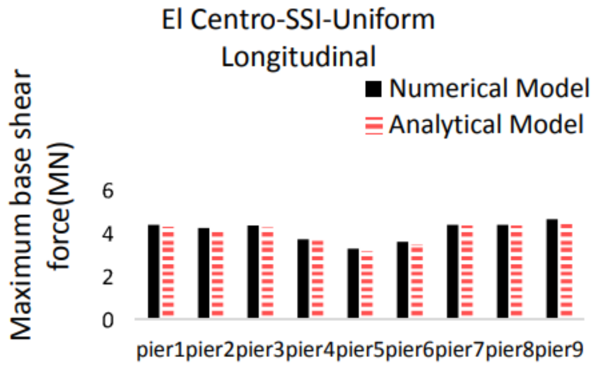

(a)

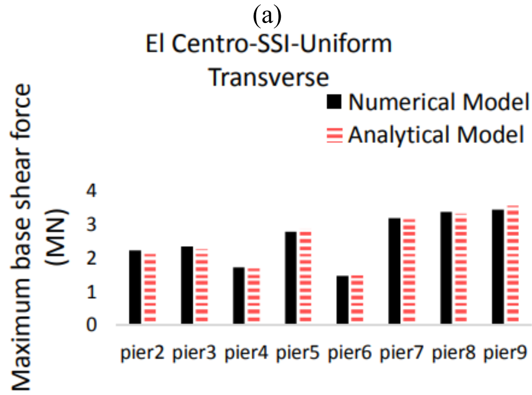

(b)

Fig. 15 Maximum base shear force for the 1979 El Centro earthquake in the (a) longitudinal and (b) transverse directions

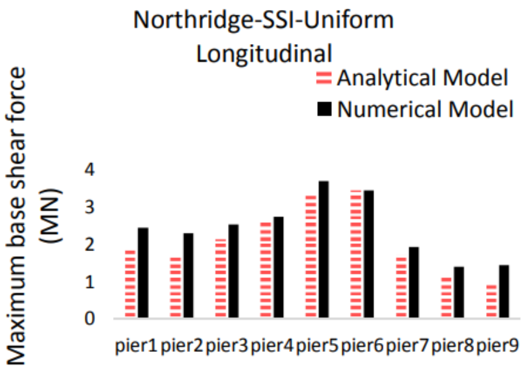

(a)

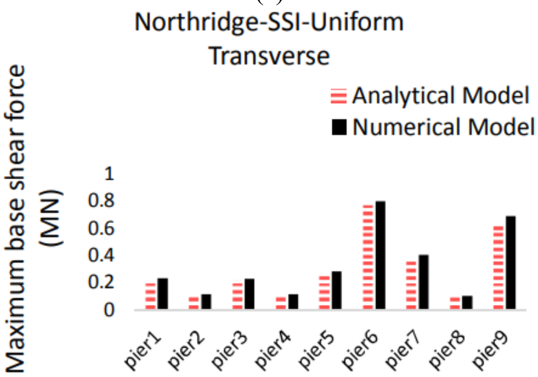

(b)

Fig. 16 Maximum base shear force for the 1994 Northridge earthquake in the (a) longitudinal and (b) transverse directions

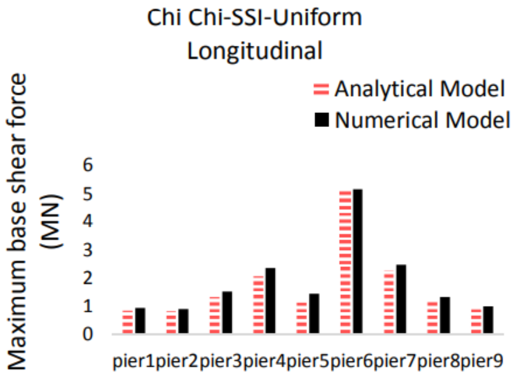

(a)

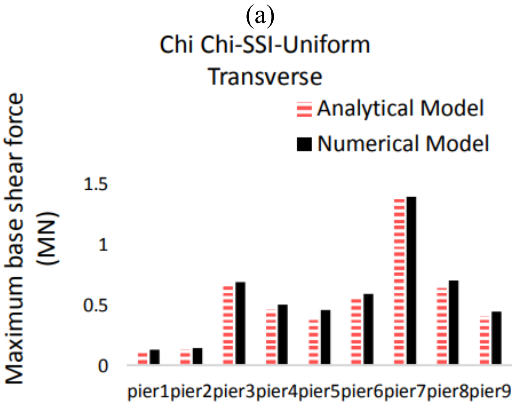

(b)

Fig. 17 Maximum base shear force for the 1999 Chi Chi earthquake in the (a) longitudinal and (b) transverse directions

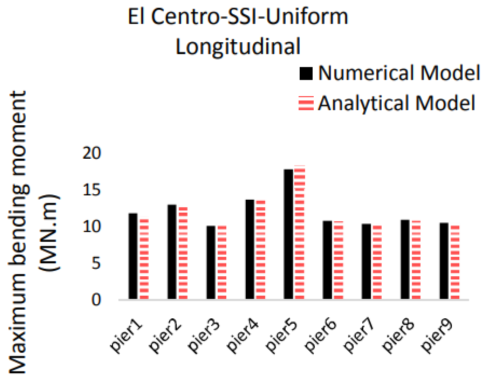

(a)

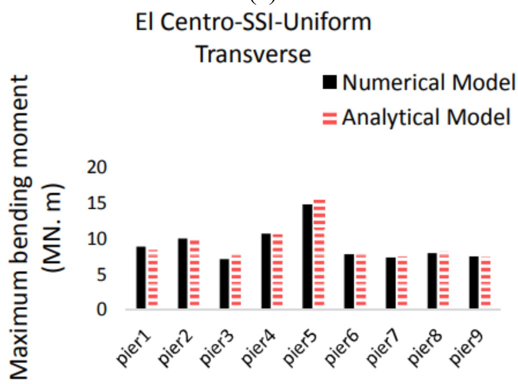

(b)

Fig. 18 Maximum bending moment for the 1979 El Centro earthquake in the (a) longitudinal and (b) transverse directions

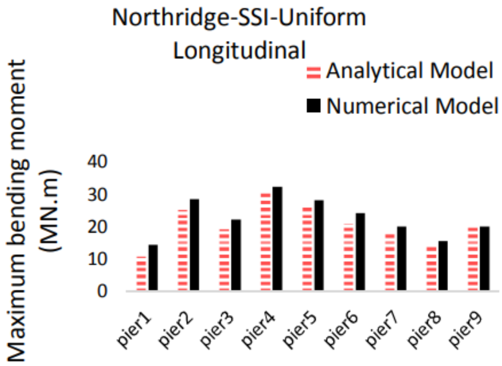

(a)

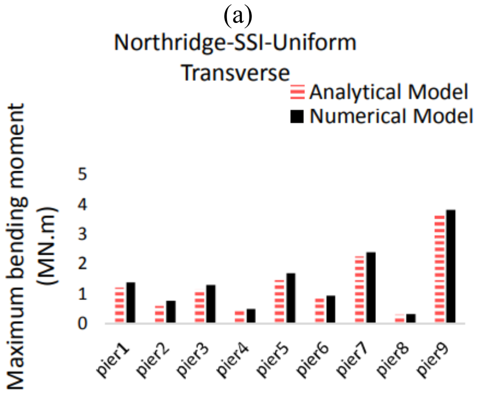

(b)

Fig. 19 Maximum bending moment for the 1994 Northridge earthquake in the (a) longitudinal and (b) transverse directions

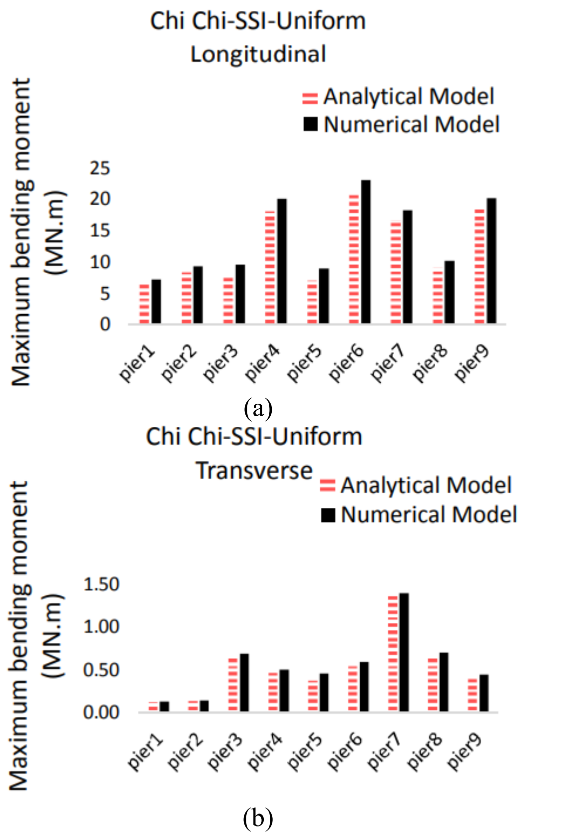

Fig. 20 Maximum bending moment for the 1999 Chi Chi earthquake in the (a) longitudinal and (b) transverse directions

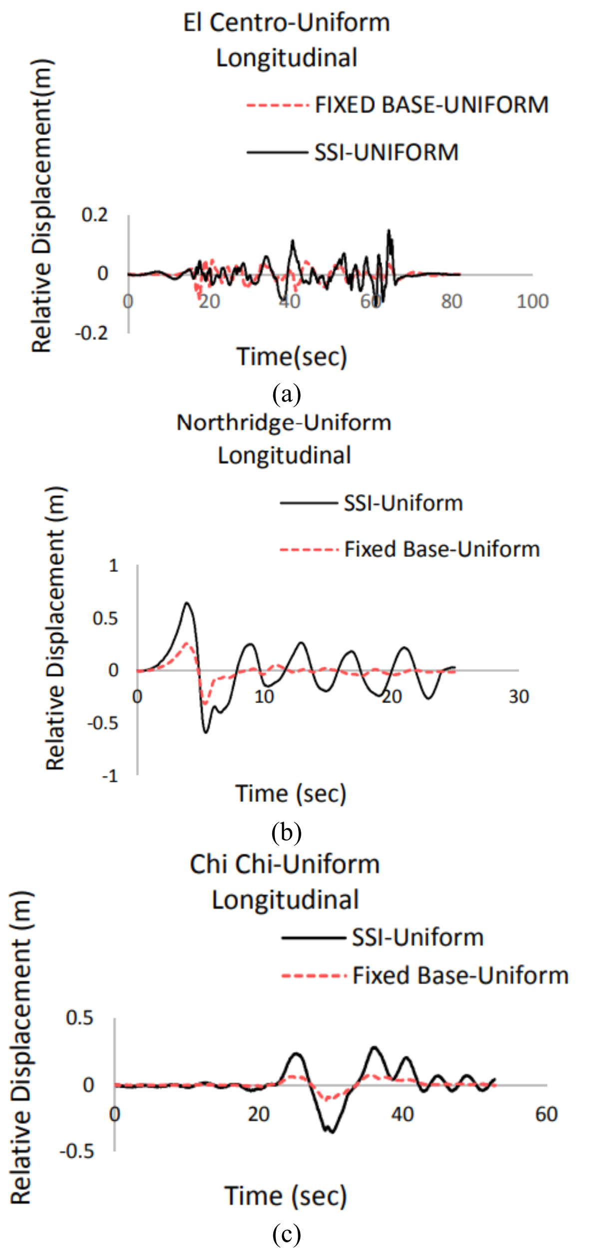

Fig. 21 The first deck relative displacements TH with respect to the ground surface for (a) the 1979 El Centro earthquake, and (b) the 1994 Northridge earthquake, and (c) the 1999 Chi Chi earthquake; comparing the responses in SSI and the fixed base models

predictions of the numerical and analytical models for the maximum base shear force and maximum bending moments for all the piers in the longitudinal and transverse directions, respectively. The analytical model generally overestimates the shear force and bending moments but it is not significant. The shear forces at the base of the piers are satisfactorily predicted in the longitudinal direction by the analytical model in the El Centro, 1979 earthquake but in the Northridge, 1994 and Chi Chi, 1999 earthquake longitudinal shear force is about 23% and 17% overestimated, respectively. In the transverse direction, the base shear forces are more exactly predicted by the analytical model. Similar observations are noted when comparing the maximum base bending moments. The relative difference in estimation of the maximum shear forces varies in the range of about 0-12%, 2-37% and 1-22% in longitudinal and 0-8%, 2-23% and 1-18% in transverse directions for the El Centro, Northridge and Chi Chi earthquake, respectively in the different piers. The relative difference in estimating the maximum bending moments varies in the range of about 0-19%, 5-33% and 0-28% about the transverse axis and 0-10%, 2-14% and 0-10% about the longitudinal axis for the El Centro, Northridge and Chi Chi earthquake, respectively in the different piers. Actually, the differences between the results of the analytical and numerical models occurs because in the analytical model the SSI effect is simulated by springs and dashpots and when the soil and foundation responses are highly nonlinear hysteretic, these elements appear not to be suitable to represent the seismic response of the foundation system of the bridge. Also, in relative low intensity or far field earthquakes, the results show that the analytical model can suitably predicts the seismic responses of the bridge. It occurs because seismic performance of a structural system depends on its natural vibration periods which depend on the stiffness and mass of the system.

In this analytical method, the nonlinear hysteretic response of soil and its interaction with the bridge structure is presented by constant stiffness at the base of the piles and cap levels. The secant values along the piles are concentrated at the end of the piles by use of the proper shape functions. The secant stiffness which were derived by

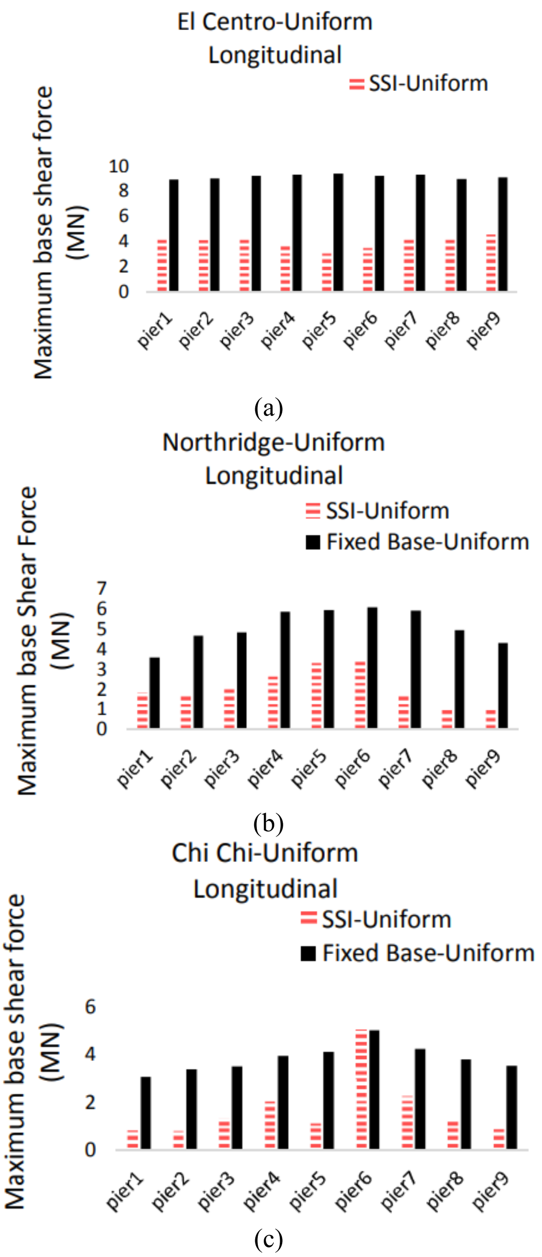

Fig. 22 Maximum base shear force for (a) the 1979 El Centro earthquake, and (b) the 1994 Northridge earthquake, and (c) the 1999 Chi Chi earthquake; comparing the responses in the SSI and the fixed base models

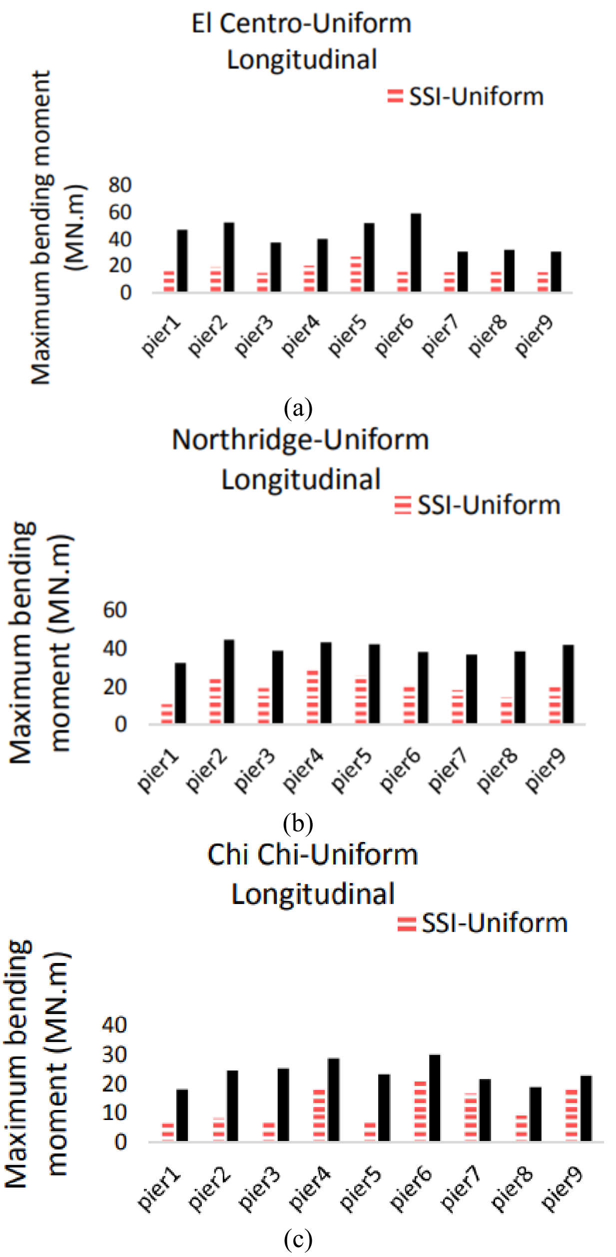

Fig. 23 Maximum bending moment for (a) the 1979 El Centro earthquake, and (b) the 1994 Northridge earthquake, and (c) the 1999 Chi Chi earthquake; comparing the responses in the SSI and the fixed base models

this method can make proper modeling of seismic SSI in far field earthquakes. Although, this proposed model is more capable in transverse direction. It means that natural vibration periods are more exactly calculate in the transverse direction and so seismic responses are truly predicted in this direction. To emphasize the relative importance of the soil-structure interaction, fixed base model of the considered bridge is simulated in the ABAQUS. In this model soil medium and pile group foundations are removed and all of the piers are made fixed at the base. Fig. 21 shows the computed time histories of the first deck relative displacement with respect to the piers base using the SSI and fixed base analytical models in longitudinal direction. As can be observed, displacements determined from the SSI model are significantly larger than those for fixed base model in every three events. Maximum difference between the results is about 43%, 59% and 48% for the El Centro, Northridge and Chi Chi earthquake, respectively. Maximum base shear farce and maximum moments for the piers are also compared for the SSI effect (Fig. 22 and Fig. 23). Opposite to the variation of the displacement responses, the maximum base shear and bending moment responses determined from the analysis cases including the SSI effect are much larger than the responses obtained from the fixed base model, which neglects the SSI effect. The range of variation between the

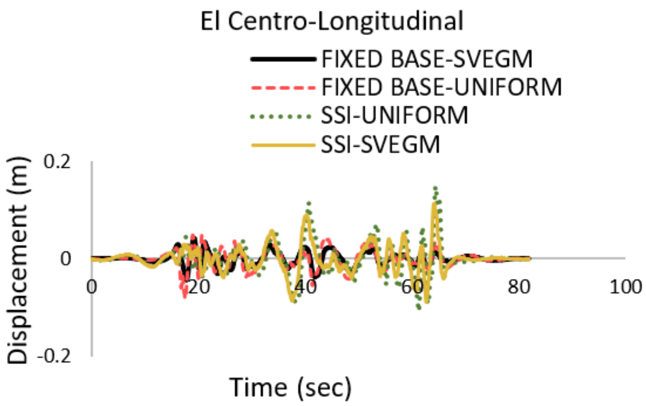

Fig. 24 The first deck relative displacements TH with respect to the ground surface for the 1979 El Centro earthquake, comparing the responses including and excluding SSI and SVEGM effects

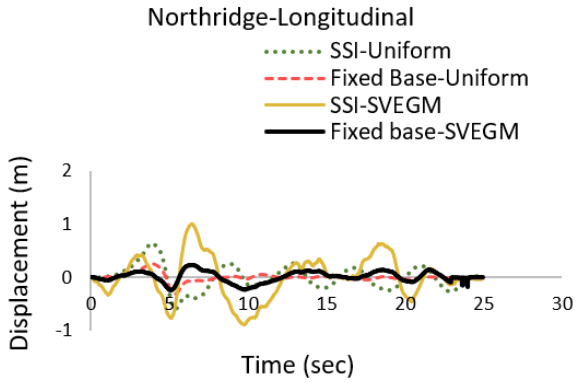

Fig. 25 The first deck relative displacements TH with respect to the ground surface for the 1999 Chi Chi earthquake, comparing the responses including and excluding SSI and SVEGM effects

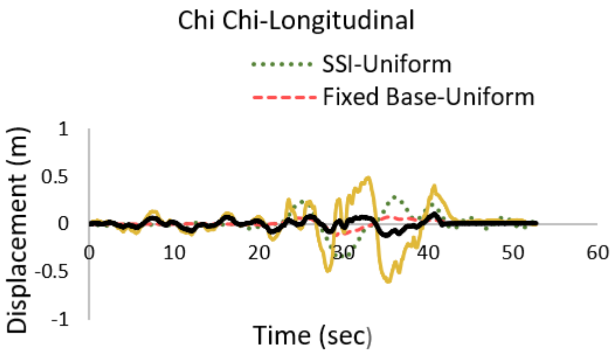

Fig. 26 The first deck relative displacements TH with respect to the ground surface for the 1994 Northridge earthquake, comparing the responses including and excluding SSI and SVEGM effects

results for maximum base shear forces are about 48-62%, 42-78%, and 5-69% for the El Centro, Northridge and Chi Chi earthquakes, respectively in longitudinal direction. Also, the range of variation for maximum bending moments are about 50-120%, 48-152%, and 12-137% for the El Centro, Northridge and Chi Chi earthquake, respectively about the transverse axis. The results imply that the effect of the soil-structure interaction on the seismic responses is more obvious in taller piers.

The significance of the spatially varying earthquake ground motions on the dynamic bridge responses including and excluding the SSI effect are determined by the analytical model because non-uniform ground motions are determined at piers location by the SIMQKE record generator and so cannot be applied in the numerical continuum model. The first deck relative displacements with respect to the ground surface obtained for the specified ground motion cases are compared in Figs. 24-26. It is apparent that the dynamic deck displacements calculated for the SVEGM and SSI effects are larger than those for the remaining cases in longitudinal direction. This effect is more obvious in near-field ground motions (e.g. the Northridge and Chi Chi earthquakes). It is also obvious that the fixed base models induce the smallest displacements. The SVEGM effect causes 10% and 23% larger displacements than those of the uniform excitation for the Northridge and Chi Chi earthquakes, respectively and 2% smaller result for the El Centro earthquake excluding the SSI effect. In case of including SSI effect the SVEGM effect causes 43% and 25% larger displacements for the Northridge and Chi Chi events, respectively and 9% smaller displacement for the El Centro event.

8. Conclusions

In this paper, dynamic analysis of a long-span bridge subjected to spatially varying earthquake ground motion and under the effect of soil- structure interaction is performed by solving the equation of motion for the proposed model. For the first time, a new simple but capable model has been proposed to simulate the soil-pile system considering the pile foundation with distributed mass in a longitudinal bridge model.

It is obvious that the dynamic bridge responses calculated for the SSI cases are usually much larger than those excluding the effect of SSI in both longitudinal and transverse directions. In the analysis cases including SSI, SVEGM models generally include larger responses in the longitudinal direction.

If the effects of SSSI and SVEGM are considered simultaneously, it should be noticed that the results will not be as same as which obtained from the addition of the response determined from these effects separately. The effects of SSSI and SVEGM amplify each. It is also observed that considering the effect of SSI with respect to the SVEGM can change the dynamic response of long-span bridges in comparison with the cases in which only SSI effect or none of them is considered.

Results of this study show that it is necessary to include the effects of SSI and SVEGM in international standards of structural seismic design, especially for large and long structures which not considering them leads to miscalculating the seismic response of these structures.

References

AASHTO (2012), *LRFD Bridge Design Specifications*, American

Association of State High way and Transportation Officials, Washington, D.C., U.S.A.

ABAQUS (2011), *Version 6.11 User's Manual*, Dassault Systèmes Simulia Corp., Providence, Rhode Island, U.S.A.

Adanur, S., Altunisik, A.C., Soyluk, K. and Bayraktar, A. (2016), "Multiple-support seismic response of Bosporus suspension bridge for various random vibration method", *Case Stud. Struct. Eng.*, **5**, 54-67.

Apaydin, N.M., Bas, S. and Harmandar, E. (2016), "Response of the Fatih Sultan Mehmet Suspension Bridge under spatially varying multi-point earthquake excitations", *Soil Dyn. Earthq. Eng.*, **84**, 44-54.

API (2007), *Recommended Practice for Planning, Designing, and Constructing Fixed Offshore Platforms*, American Petroleum Institute, Washington, U.S.A.

Battini, J.C. (2006), Structural Dynamics, Royal Institute of Technology (KTH), Stockholm, Sweden, <http://www2.mech.kth.se/~jean//dynamics.html>.

Bi, K., Hao, H. and Chouw, N. (2011), "Influence of ground motion spatial variation, site condition and SSI on the required separation distances of bridge structures to avoid seismic pounding", *Earthq. Eng. Struct. Dyn.*, **40**, 1027-1043.

Carbonari, S., Morici, M., Dezi, F., Gara, F. and Leoni, G. (2017), "Soil-structure interaction effects in single bridge piers founded on inclined pile groups", *Soil Dyn. Earthq. Eng.*, **92**, 52-67.

Chi, Y., Yu, M., Huang, L. and Xu, L. (2017), "Finite element modeling of steel-polypropylene hybrid fiber reinforced concrete using modified concrete damaged plasticity", *Eng. Struct.*, **148**, 23-35.

Datta, T.K. (2010), *Seismic Analysis of Structures*, John Wiley & Sons (Asia) Pte Ltd, 2 Clementi Loop, 02-01, Singapore.

Davoodi, M., Jafari, M.K. and Sadreddini, A. (2013), "Effect of multi-support excitation on seismic response of embankment dams", *Int. J. Civ. Eng.*, **11**(1), 19-28.

Davoodi, M., Razmkhah, A. and Javaheri, A. (2012), "Considering the effects of SVEGM on dynamic stress-strain distribution of embankment dams", *Civ. Eng. Infrastruct. J.*, **45**, 529-541.

Drucker, D.C. and Prager, W. (1952), "Soil mechanics and plastic analysis for limit design", *Quart. Appl. Math.*, **10**(2), 157-165.

Drygala, I.J., Dulinska, J.M. and Wazowski, M. (2017), "Seismic performance of a cable-stayed footbridge using a concrete damage plasticity model", *Proc. Eng.*, **193**, 525-532.

EduPro Civil Systems Inc (2003), *ProShake, version 1.12*, Sammamish, Washington, U.S.A., <http://www.proshake.com>.

GEOSPECTRA (1997), *A Division of Kleinfelder, Inc. Design Manual*, *Foundation Stiffnesses under Seismic Loading*, Washington State Department of Transportation, U.S.A.

Ghanbari, A., Khalilpasha, A., Sabermahani, M. and Heydari, B. (2013), "An analytical technique for estimation of seismic displacements in reinforced slopes based on horizontal slices method (HSM)", *Geomech. Eng.*, **5**(2), 143-164.

Hany, F.N., Hantouche, E.G. and Harajli, M.H (2016), "Finite element modeling of FRP-Confined concrete using modified concrete damaged plasticity", *Eng. Struct.*, **125**, 1-14.

Hoseini, S.S., Ghanbari, A. and Davoodi, M. (2017), "Evaluation of long bridges dynamic responses under the effect of spatially varying earthquake ground motion", *Bridge Struct.*, **13**(1), 25-42.

Ilankatharan, M. and Kutter, B. (2008), "Numerical simulation of a soil model-model container-centrifuge shaking table system", *Proceedings of the Geotechnical Earthquake Engineering and Soil Dynamics IV*, Sacramento, California, U.S.A., May.

Karmakar, D., Ray-Chaudhuri, S. and Shinozuka, M. (2012), "Seismic response evaluation of retrofitted Vincent Thomas Bridge under spatially variable ground motions", *Soil Dyn. Earthq. Eng.*, **42**, 119-127.

Kwon, O.S. and Elnashai, A.S. (2008), "Seismic analysis of Meloland road overcrossing using multiplatform simulation software including SSI", *J. Struct. Eng.*, **134**(4), 651-660.

Lee, S., Feng, M.Q., Kwon, S.J. and Hong, S.H. (2011), "Equivalent modal damping of short-span bridges subjected to strong motion", *J. Bridge Eng.*, **16**(2), 316-323.

Lubliner, J., Oliver, J., Oller, S. and Onate, E. (1989), "A plastic-damage model for concrete", *Int. J. Solids Struct.*, **25**(3), 299-329.

Maedeh, P.A., Ghanbari, A. and Wu, W. (2017), "New coefficients to find natural period of elevated tanks considering fluid-structure-soil interaction effects", *Geomech. Eng.*, **12**(6), 701-717.

Mander, J., Priestley, M. and Park, R. (1988), "Theoretical stress-strain model for confined concrete", *J. Struct. Eng.*, **114**(8), 1804-1826.

Nazmy, A.S. and Abdel-Ghaffar, A.M. (1992), "Effects of ground motion spatial variability on the response of cable-stayed bridges", *Earthq. Eng. Struct. Dyn.*, **21**(1), 1-20.

Pacheco, G. (2007), "Dynamic lateral response of single piles considering soil inertia contribution", Ph.D Dissertation, University of Puerto Rico, Puerto Rico.

Pulinska, J.M. and Czerba, R.S. (2013), "Assessment of concrete bridge performance under moderate seismic shock using concrete damage plasticity model", *Proc. Eng.*, **57**, 1319-1328.

Rahmani, A., Taiebat, M., Finn, W.D.L. and Ventura, C.E. (2016), "Evaluation of substructuring method for seismic soil-structure interaction analysis of bridges", *Soil Dyn. Earthq. Eng.*, **90**,112-127.

Seed, H. and Idriss, I. (1970), "Soil moduli and damping factors for dynamic response analyses", Technical report EERC 70-10, Earthquake Engineering Research Center, University of California, Berkeley, California, U.S.A.

Sextos, A.G., Pitilakis, K.D. and Kappos, A.J. (2003), "Inelastic dynamic analysis of RC bridges accounting for spatial variability of ground motion, site effects and soil-structure interaction phenomena. Part 1: Methodology and analytical tools", *Earthq. Eng. Struct. Dyn.*, **32**(4), 607-627.

Sextos, A.G., Pitilakis, K.D. and Kappos, A.J. (2003), "Inelastic dynamic analysis of RC bridges accounting for spatial variability of ground motion, site effects and soil-structure interaction phenomena. Part 2: parametric study", *Earthq. Eng. Struct. Dyn.*, **32**(4), 629-652.

Shirgir, V., Ghanbari, A. and Shahrouzi, M. (2016), "Natural frequency of single pier bridges considering soil-structure interaction", *J. Earthq. Eng.*, **20**(4), 611-632.

Soyluk, K. and Sicacik, E.A. (2012), "Soil-structure interaction analysis of cable-stayed bridges for spatially varying ground motion components", *Soil Dyn. Earthq. Eng.*, **35**, 80-90.

Sun, J., Golesorkhi, R. and Seed, H. (1988), Dynamic moduli and damping ratios for cohesive soils. Technical report EERC 88-15, Earthquake Engineering Research Center, University of California, Berkeley, California, U.S.A.

Varzaghani, M.I. and Ghanbari, A. (2014), "A new analytical model to determine dynamic displacement of foundations adjacent to slope", *Geomech. Eng.*, **6**(6), 561-575.

Wang, J., Carr, A.J., Cooke, N. and Moss, P.J. (2009), "The response of a 344 m long bridge to non-uniform earthquake ground motions", *Eng. Struct.*, **31**(11), 2554-2567.

Werner, S. (1993), "Study of Caltrans; seismic evaluation procedures for short bridge over crossing structures", Technical Report 59Q122, California Department of Transportation Division of Structures, Sacramento, California, U.S.A.

CC